Energy-dependent charge-changing cross sections and proton distribution of ^{28}Si

T. Yamaguchi,[1,*] M. Fukuda,[2] S. Fukuda,[3] G. W. Fan,[4] I. Hachiuma,[1] M. Kanazawa,[3] A. Kitagawa,[3] T. Kuboki,[1] M. Lantz,[5] M. Mihara,[2] M. Nagashima,[6] K. Namihira,[1] D. Nishimura,[2] Y. Okuma,[6] T. Ohtsubo,[6] S. Sato,[3] T. Suzuki,[1] M. Takechi,[5] and W. Xu[4]

[1]*Department of Physics, Saitama University, Saitama 338-8570, Japan*
[2]*Department of Physics, Osaka University, Osaka 560-0043, Japan*
[3]*National Institute of Radiological Sciences, Chiba 263-8555, Japan*
[4]*Shanghai Institute of Applied Physics, Jiading Shanghai, 201800, People's Republic of China*
[5]*RIKEN Nishina Center, Wako, Saitama 351-0198, Japan*
[6]*Department of Physics, Niigata University, Niigata 950-2181, Japan*

(Received 27 April 2010; published 12 July 2010)

The charge-changing cross sections (σ_{cc}) of ^{28}Si on a carbon target were measured with high precision at intermediate energies from 100 to 600 MeV/nucleon. The measured σ_{cc} decreases rapidly from low energies up to 200 MeV/nucleon, whereas at higher energies it appears almost constant. The energy dependence of σ_{cc} is compared with a Glauber-type model calculation where only the proton distribution of ^{28}Si is taken into account. A phenomenological correction factor deduced from the present data satisfactorily reproduces the experimental σ_{cc} for other stable nuclei, whose charge distributions were determined by electron scattering and muon capture experiments.

DOI: 10.1103/PhysRevC.82.014609 PACS number(s): 21.10.Ft, 25.70.Mn, 27.30.+t

I. INTRODUCTION

Charge-changing cross sections, σ_{cc}, of energetic heavy ions are of interest for various research fields. Systematic data compilation allows the development of models and empirical formulas to predict the cross sections. These models and formulas have applications in studies of radiation protection issues including radiation shields for accelerators, reactors, and spacecraft, and in heavy-ion cancer therapy [1]. Charge-changing cross sections are also important to understand the origin, acceleration mechanism, and propagation of high-energy galactic cosmic rays. Heavy-ion synchrotrons at laboratories such as LBL, CERN, BNL, GSI, and the Heavy Ion Medical Accelerator (HIMAC) are the main providers of the cross-section data. A number of systematic measurements were performed using a range of ions on various targets (see, e.g., Refs. [2–4] and references therein).

For fundamental nuclear physics purposes, such systematics have clarified the reaction mechanisms in heavy-ion collisions. For example, Scheidenberger *et al.* showed a significant effect of the electromagnetic interaction in the charge-changing and pickup cross sections for lead ions at ultrarelativistic energies [5]. However, from a nuclear structure point of view, relatively little information has been gleaned from σ_{cc} of heavy ions.

In peripheral collisions, the charge-changing cross section may in a simple picture reflect the collision probability of the valence proton(s) of the projectile with the target nucleus, and thus be sensitive to the (point-)proton distribution, particularly for neutron-rich projectiles. Chulkov *et al.* measured σ_{cc} for neutron-rich unstable nuclei from boron to fluorine isotopes at a relativistic energy at GSI [6]. They found that σ_{cc} stays constant among the isotopes in each element. Because their nuclear matter radii increase toward the neutron drip line, the data suggest that only the valence neutrons that are added to the core nuclei contribute to the enlargement of the matter radii, and the proton distributions remain unperturbed even near the neutron drip line. Meng *et al.* calculated the charge and matter density distributions of neutron-rich nuclei (carbon to fluorine) in the relativistic continuum Hartree-Bogoliubov theory and applied the calculated densities to a Glauber-type calculation of the charge-changing cross sections [7]. The results provide a picture of the evolution of neutron skin structure in which the charge-changing cross sections of heavy ions at intermediate energies can be closely related to their proton distributions. Bochkarev *et al.* also found evidence for the neutron skin in ^{20}N using a combined analysis of the interaction and charge-changing cross sections [8]. Their analysis, however, only gives the upper limit of the radius for the proton distribution. The relation between the radius, r_p, and the charge-changing cross section, σ_{cc}, still must be investigated in detail. In this regard, precise measurements of σ_{cc} of a nucleus whose charge distribution is experimentally known could be particularly valuable.

In the present study, we measured with high precision the charge-changing cross sections, σ_{cc}, of ^{28}Si on carbon at intermediate energies ranging from 100 to 600 MeV/nucleon. Since the charge distribution of ^{28}Si is well known, a detailed study based on a Glauber-type model calculation can be performed. The paper describes the present experiment and introduces a phenomenological way to relate r_p to σ_{cc}.

II. EXPERIMENT AND ANALYSIS

The measurements were performed using the fragment separator [9] at the synchrotron facility HIMAC (Chiba,

*yamaguti@phy.saitama-u.ac.jp

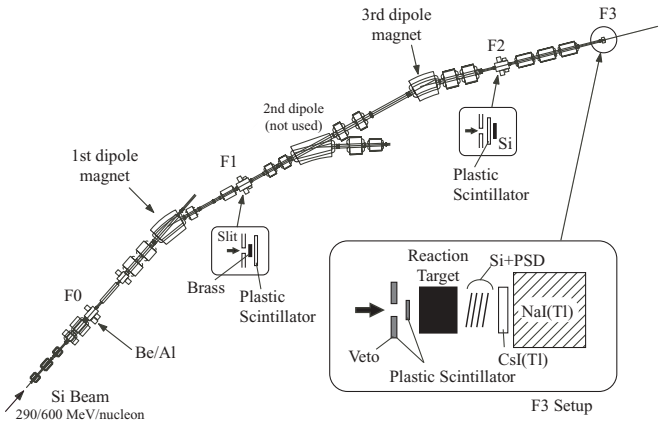

FIG. 1. Schematic drawing of the fragment separator. The inset shows the experimental setup around the reaction target at the F3 focal plane (not to scale).

Japan). A primary beam of ^{28}Si with two energies, 290 and 600 MeV/nucleon, was used. To change the beam energy in the range from 100 to 600 MeV/nucleon, several materials were installed as energy degraders at the production-target port (F0) and the first focal plane (F1) in the separator beam line as shown in Fig. 1. Data sets I–VI, shown in Table I, were taken with the 600-MeV/nucleon primary beam, and data sets VII–XI at the 290 MeV/nucleon beam. The combination of degrader materials used is shown in Table I.

The principle of the experiment is the transmission method. The charge-changing cross section, σ_{cc}, is derived from the equation

$$\sigma_{cc} = -\frac{1}{t}\ln\left(\frac{\Gamma}{\Gamma_0}\right), \quad (1)$$

where Γ and Γ_0 represent the counting ratio of the particles with $Z = 14$ relative to incoming ^{28}Si for a target-in and target-out run, respectively, and t denotes the target thickness (i.e., the number of nuclei per unit area). The carbon target was positioned at the third focal plane (F3). The target thickness in each run is listed in Table I. The variation in thickness is approximately 5 μm, which is added in quadrature to the total error as a systematic uncertainty.

TABLE I. Experimental conditions.[a]

Data set	F0 material (thick/mm)	F1 material (thick/mm)	E_{in} (MeV/nucleon)	Carbon t (g/cm^2)
I			587	4.506
II	Al (15)		527	4.506
III	Al (23)		494	4.506
IV	Be (8)	Brass (10)	454	4.506
V		Brass (20)	359	4.506
VI	Al (23)	Brass (15)	310	4.506
VII			272	3.597
VIII				2.227[b]
IX	Be (8)		239	4.126
X	Al (15)		178	1.900
XI	Al (23)		110	0.8301

[a]Degrader materials with thickness at F0 and F1, beam energies in front of the target (E_{in}), and thickness of carbon (t) are given.
[b]Obtained by subtracting data set X from data set IX.

A schematic drawing of the experimental setup around the reaction target is shown in the inset of Fig. 1. Upstream of the carbon target, each incident ^{28}Si beam particle was identified by the standard $B\rho$-ΔE-time-of-flight (TOF) technique to avoid any contaminants produced at the degrader materials. The energy-loss analysis, ΔE, was performed using a silicon detector (500 μm thick) at the second focal plane (F2). Two sets of plastic scintillation counters (2 and 0.5 mm thick) placed at the F1 and F3 focal planes, respectively, provided the time-of-flight information. The F3 plastic scintillation counter (20×20 mm^2) was used to trigger the data acquisition. To avoid pileup of the counter telescope downstream of the reaction target, another plastic scintillator (1 mm thick) with a ϕ19-mm hole in the center on the beam-line axis was used as a veto in front of the target. Using the F3 and veto plastic scintillation counters, the events occurring within a 10-μs time gate were recorded as pileup and rejected in the offline analysis. To change the beam energies, relatively thick materials were employed. Neutron removal reactions in the degraders might produce other Si isotopes as main contaminants, which could only be resolved by the time of flight. Full particle identification ensured the contaminations of such fragments were negligibly small.

Downstream of the target, a stack of three silicon detectors (50×50 mm^2, 500 μm thick each) and a charge-division readout position-sensitive detector (PSD; 50×50 mm^2, 500 μm thick) measured ΔE of the outgoing particles. The position distributions measured by the PSD ensured an acceptance for the particles with $Z = 14$ penetrating through all the silicon detectors. A NaI(Tl) scintillation counter (ϕ4 in., 70 mm thick) measured the total energy in the lower energy settings.

In the analysis of data sets I–VI, a sum of ΔE from the silicon detectors unambiguously identified the charge of the outgoing particles. A typical ΔE spectrum in data set I is shown in Fig. 2(a), with 2.1% resolution in $\Delta Z/Z$ [full width at half maximum (FWHM)]. For data sets VII–XI, the Si-NaI(Tl) telescope made possible a ΔE-E measurement. A ΔE-E spectrum in data set IX is shown in Fig. 2(b). A clear Z separation was obtained with both methods. It should be noted

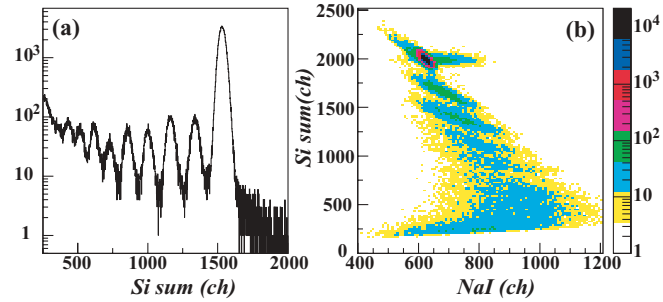

FIG. 2. (Color online) (a) Typical ΔE spectrum of the stack detector in data set I. The sum of three silicon detectors and the position-sensitive detector is plotted. (b) A ΔE-E spectrum in data set IX. Both methods allow a clear separation of the particles with $Z = 14$ from other fragments.

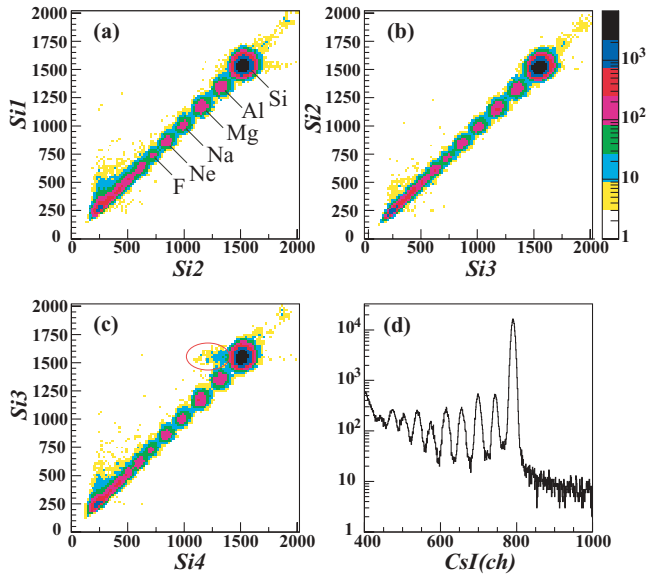

FIG. 3. (Color online) Typical two-dimensional correlation plots of each silicon detector: (a) Si1 to Si2, (b) Si2 to Si3, (c) Si3 to Si4(PSD), and (d) a typical ΔE spectrum observed by the CsI(Tl) scintillation counter (data set I). The resolution is 1.7% in $\Delta Z/Z$ (FWHM).

that in the ΔE-E method the beam energies in the target-out runs were adjusted by changing the degrader thickness so that the energies just in front of the NaI(Tl) detector would be the same as those in the target-in runs. The main reason for this is that the particles entering the NaI(Tl) detector have a long range, giving a large reaction probability in the detector itself. This reaction probability is energy dependent, giving a different background ratio Γ_0 for different energies. Therefore, the energy has to be adjusted in the target-out runs so that Γ_0 gives the proper correction for the false reaction events.

All of the silicon detectors were angled at 6° with respect to the focal plane to minimize channeling events. A channeling effect makes a smaller energy deposit into the detectors, resulting in a low-energy tail in the ΔE spectra. Such an effect might lead to counting loss and false cross sections. The fraction of channeling events was very small, as seen in Fig. 3. In Figs. 3(a)–3(c), two-dimensional correlation plots are shown for all silicon detectors in the case of data set I. The channeling events were mainly seen in the fourth detector (Si4), shown by the (red) ellipse in Fig. 3(c), but were less than 0.5% of the total. Because the beam emittances at the stack detector in the target-in runs could be different from those in the target-out runs owing to the energy-loss processes in the beam-line materials and the carbon targets, a possible asymmetry of channeling events between Γ and Γ_0 might occur. An asymmetry was thus estimated to be less than 0.3% in data sets I–VI. In data sets VII–XI, the channeling events were mainly caused by the second silicon detector (Si2). The amount of channeling events was larger than in data sets I–VI, but always less than 1%, and the asymmetry was estimated to be less than 0.7%. Although the channeling events were clearly identified, these asymmetry effects might be a possible source of uncertainty and thus were included in the total error.

The reaction events in the stack detector, which generally give larger pulse heights than those of the projectiles, were included as noninteracting events in the carbon targets in the analyses of Γ and Γ_0. The Γ and Γ_0 without the reaction events also gave the consistent results.

The event selection condition in the ΔE and ΔE-E spectra might introduce an uncertainty in the charge-changing cross sections. This was confirmed to be less than 0.3% for data sets I–VI and 1% for data sets VII–IX by changing the gate width applied in the spectra. All uncertainties mentioned above were added in quadrature to the total error.

In addition to the stack detector, a 5-mm-thick CsI(Tl) scintillation counter was placed to perform a ΔE analysis redundantly. The ΔE resolution was comparable to that of the stack detector [1.7% in $\Delta Z/Z$ (FWHM); see Fig. 3(d)].

III. RESULTS AND DISCUSSION

The results of the charge-changing cross sections are listed in Table II and shown graphically in Fig. 4. The cross sections from other experiments are also plotted [2,10,11]. The present results are consistent with the previous data [10,11]. In general, the charge-changing cross sections appear almost constant above 200 MeV/nucleon and increase rapidly below 200 MeV/nucleon as the energy decreases.

To investigate the relation between the radius for the proton distribution and the charge-changing cross sections, we performed a zero-range optical-limit Glauber calculation [12]. The reaction cross section σ_R is described by the following equations:

$$\sigma_R = 2\pi \int b[1 - T(b)]\, db, \tag{2}$$

$$T(b) = \exp\left[- \sum_{i,j} \sigma_{ij} \rho^z_{\mathrm{targ}}(s) \rho^z_{\mathrm{proj}}(|b - s|) ds \right], \tag{3}$$

where b denotes the impact parameter, σ_{ij} denotes the nucleon-nucleon cross sections, and ρ^z_{targ} (ρ^z_{proj}) is the z-integrated

TABLE II. Results of σ_{cc} of ^{28}Si on C.[a]

Data set	E_{mid} (MeV/nucleon)	^{28}Si + C		Analysis method
		σ_{cc} (mb)	Error (mb)	
I	550	1124	7	ΔE
II	488	1124	6	ΔE
III	453	1114	6	ΔE
IV	412	1103	7	ΔE
V	309	1119	8	ΔE
VI	255	1119	6	ΔE
VII	225	1117	7	ΔE-E
VIII	208	1138[b]	17	
IX	175	1164	12	ΔE-E
X	144	1195	12	ΔE-E
XI	90	1292	25	ΔE-E

[a]Beam energies at the middle of the target (E_{mid}) and charge-changing cross sections (σ_{cc}) with their total errors are given in millibarns (mb).
[b]Obtained by subtracting data set X from data set IX.

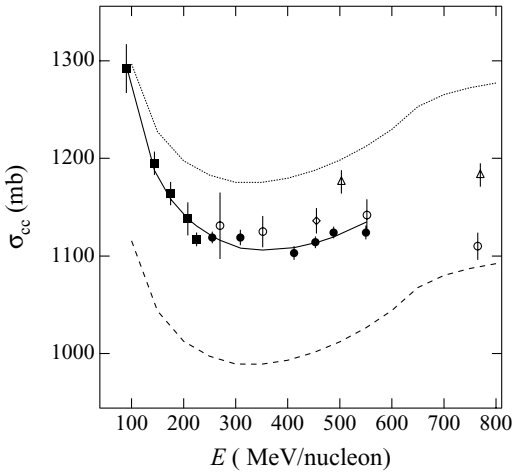

FIG. 4. Energy dependence of σ_{cc} of ^{28}Si on C. The present data are represented by solid circles (data sets I–VI) and solid squares (VI–IX). Other experimental values are shown by open triangles [2], open circles [10], and an open diamond [11]. The dotted curve represents the energy dependence of σ_R of ^{28}Si on C calculated by a zero-range optical-limit Glauber model. The dashed curve shows the same Glauber-type calculation but only the proton distribution of ^{28}Si is taken into account. The solid curve is the same as the dashed curve but with a phenomenological correction factor $\mathcal{E}(E)$ included to reproduce the data.

density distribution of the target (projectile). $T(b)$ is called the transmission function.

Following Bhagwat and Gambhir [13], $T(b)$ is resolved into two parts:

$$T(b) = T^p(b)T^n(b), \tag{4}$$

$$T^p(b) = \exp\left[-\left(\sigma_{pp}\int \rho_p^{\rm targ}\rho_p^{\rm proj} + \sigma_{np}\int \rho_n^{\rm targ}\rho_p^{\rm proj}\right)\right], \tag{5}$$

$$T^n(b) = \exp\left[-\left(\sigma_{pn}\int \rho_n^{\rm targ}\rho_n^{\rm proj} + \sigma_{nn}\int \rho_n^{\rm targ}\rho_n^{\rm proj}\right)\right], \tag{6}$$

where p (n) denotes the proton (neutron) contribution and proj (targ) the projectile (target) contribution. For example, $\rho_p^{\rm targ}$ is the proton density in the target nucleus, $\rho_n^{\rm proj}$ is the neutron density in the projectile nucleus, and so on. Thus, $T(b)$ consists of separate projectile-proton and projectile-neutron contributions. If we assume that the contribution from inelastic scattering is negligible at the high-energy limit [14], then the reaction cross section is nearly equal to the interaction cross section, σ_I, and is described as a sum of the charge-changing cross section, σ_{cc}, and neutron-removal cross section, σ_{-xn}:

$$\sigma_R \approx \sigma_I \tag{7}$$

$$= \sigma_{cc} + \sigma_{-xn} \tag{8}$$

$$= \tilde{\sigma}_{cc} + \tilde{\sigma}_{-xn} + \sigma_{\rm cross}, \tag{9}$$

where the proton ($\tilde{\sigma}_{cc}$), neutron ($\tilde{\sigma}_{-xn}$), and cross-term ($\sigma_{\rm cross}$) contributions are represented as

$$\tilde{\sigma}_{cc} = 2\pi\int b[1 - T^p(b)]\,db, \tag{10}$$

$$\tilde{\sigma}_{-xn} = 2\pi\int b[1 - T^n(b)]\,db, \tag{11}$$

$$\sigma_{\rm cross} = -2\pi\int b[1 - T^p(b)][1 - T^n(b)]\,db. \tag{12}$$

It should be noted that the charge-changing cross section cannot be correctly described by only the proton distribution; the cross term is also necessary ($\tilde{\sigma}_{cc} \neq \sigma_{cc}$). Bhagwat and Gambhir introduced a factor into a Glauber-type calculation to parametrize the cross term from the neutron distribution [13].

To represent σ_{cc} properly, we introduce a correction factor that modifies $\tilde{\sigma}_{cc}$ based on the presence of the cross term and additional effects such as multiple scattering and particle evaporation in the collision stage as

$$\sigma_{cc} = 2\pi\int b[1 - T^p(b)]\mathcal{E}(E)\,db, \tag{13}$$

where the phenomenological correction factor, $\mathcal{E}(E)$, is determined from precise experimental σ_{cc} data.

For the Glauber-type calculations, we use a two-parameter Fermi (2pF) distribution for ^{28}Si. In the 2pF function,

$$\rho(r) = \frac{\rho_0}{1 + \exp\left(\frac{r-R}{a}\right)}, \tag{14}$$

where the half-density radius R and the diffuseness a for the proton distribution are the parameters to be determined. The charge distribution of ^{28}Si was determined by the most recent muonic x-ray experiment [15] to be the root-mean-square charge radius $\tilde{r}_{\rm ch} = 3.123$ fm, $R_{\rm ch} = 3.1544(7)$ fm, and $a_{\rm ch} = 0.523$ fm. (The subscript ch represents the parameters for the charge distribution.) Following a recent theoretical work by Chamon *et al.* [16], the diffuseness of the proton distribution is given as $a = a_{\rm ch} - 0.03 = 0.493$ fm. The half-density radius is determined to be $R = 3.077$ fm such that the root-mean-square radius, $\tilde{r}_p$, for the proton distribution is equal to

$$\tilde{r}_p^2 = \tilde{r}_{\rm ch}^2 - \langle R_p^2\rangle - \frac{N}{Z}\langle R_n^2\rangle - \frac{3\hbar^2}{4m_p^2c^2} \tag{15}$$

where $\langle R_p^2\rangle$ and $\langle R_n^2\rangle$ are the proton [17] and neutron [18] mean-square charge radii, respectively, and the last term is the Darwin-Foldy correction.

For the target density, we use a harmonic oscillator (HO) density distribution of ^{12}C. The explicit functional form of the HO can be found in Ref. [19], where the width parameter $a_{\rm HO} = 1.645$ fm reproduces the experimental interaction cross section at 950 MeV/nucleon [19].

We first calculate the reaction cross sections of ^{28}Si on carbon. The energy dependence is shown as a dotted curve in Fig. 4. It is noted that the difference between the calculated reaction cross sections and the experimental charge-changing cross sections amounts to less than 10%, which should be attributed to the neutron-removal cross sections, according to Eq. (8).

Using the above densities, $\tilde{\sigma}_{cc}$ is calculated and shown as a dashed curve in Fig. 4. By taking the ratio of the experimental and calculated values ($\sigma_{cc}^{\rm expt}$ and $\tilde{\sigma}_{cc}^{\rm calc}$, respectively), the correction factor, $\mathcal{E}(E)$, is determined as a function of energy. We include the measured values from Refs. [10,11], since both are consistent with the present results in the energy range from

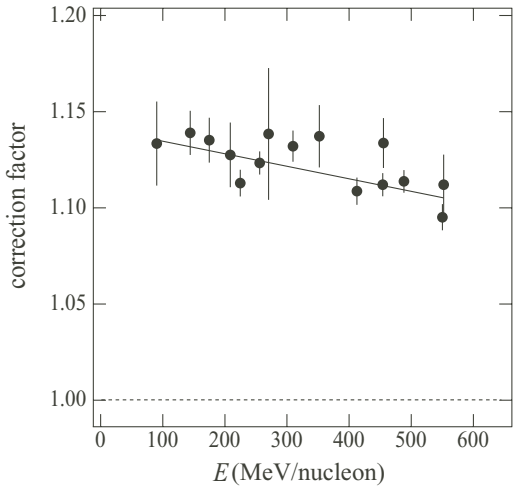

FIG. 5. Energy dependence of the correction factor $\mathcal{E}(E)$. The present data and the data from Refs. [10,11] are used in the fit over the energy range 100–600 MeV/nucleon.

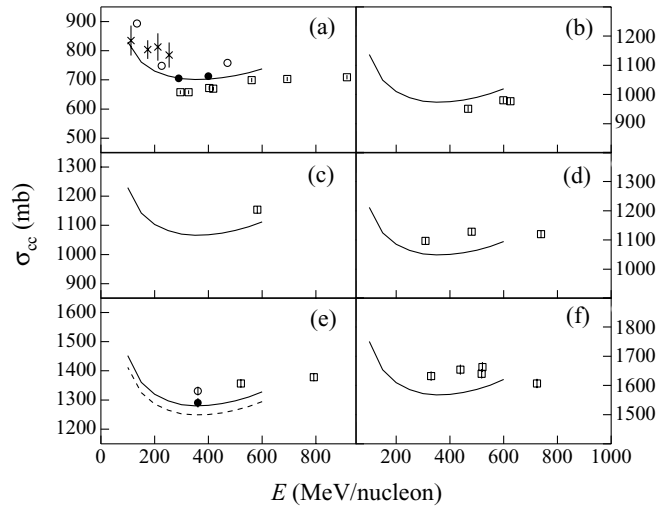

FIG. 6. Comparison of calculated charge-changing cross sections with the experimental values: (a) ^{12}C on C (open squares [2], crosses [21], open circles [22], solid circles [23]); (b) ^{20}Ne on C [2]; (c) ^{24}Mg on C [2]; (d) ^{27}Al on C [2]; (e) ^{36}Ar (solid circle [24]) and ^{40}Ar (open circle [24], open squares [2]) on C, corresponding calculations are shown in the dashed and solid curves, respectively; and (f) ^{56}Fe on C [2].

100 to 600 MeV/nucleon. The result is depicted in Fig. 5. Least-squares fitting gives the linear function

$$\mathcal{E}(E) = 1.141 - 6.507 \times 10^{-5} \times E, \qquad (16)$$

with units of MeV/nucleon in energy. The energy dependence of $\mathcal{E}(E)$ is very weak in this energy range, 200–600 MeV/nucleon. The charge-changing cross sections calculated with $\mathcal{E}(E)$ reproduce the experimental data well, as shown by the solid curve in Fig. 4.

To test the applicability of the present $\mathcal{E}(E)$ factor, the same procedure is applied to several isotopes whose charge distributions were determined experimentally. Here we select the nuclei for which the 2pF parameters are explicitly found in the literature [20]. The comparison between the predicted values (corrected Glauber calculations) and the experimental data in Ref. [2] are shown in Fig. 6, where the experimental data for ^{12}C, ^{20}Ne, ^{24}Mg, ^{27}Al, ^{40}Ar, and ^{56}Fe on C are plotted as open squares in Figs. 6(a)–6(f), respectively. In these calculations, the effects of the ground-state deformations are not included. The calculated cross sections are greater than the experimental values for ^{12}C and ^{20}Ne, but they underpredict the data for ^{24}Mg, ^{27}Al, ^{40}Ar, and ^{56}Fe. The differences between the experimental and predicted values are found to be approximately 4%, which corresponds to the precision of the $\tilde{r}_p$ determination of 4% in the present mass region. The data for ^{12}C in Refs. [21,22] also agree with the predicted values fairly well, as shown in Fig. 6(a) (crosses and open circles). Recently, the charge-changing cross sections of ^{12}C on C were measured with good precision by Zeitlin *et al.* [23], as were the charge-changing cross sections of ^{36,40}Ar on C by Iancu *et al.* [24]. The results are shown in Figs. 6(a) (solid circles) and 6(e) (solid and open circles), respectively. The ^{12}C data [23] are in excellent agreement with the calculations, with the differences found to be approximately 1%. As a typical case, the experimental σ_{cc} of ^{36}Ar, 1290.8(16.1) mb [24], is compared with the predicted value of 1249(5) mb, where $\tilde{r}_p$ of 3.217(16) fm obtained from the measured $\tilde{r}_{ch}$ of 3.327(15) fm [20] is applied in the calculation. The difference of σ_{cc} is $-3.2 \pm 1.3\%$. To reproduce the experimental σ_{cc} by the present method the other way around, $\tilde{r}_p$ is found to be 3.337(46) fm, which has a difference of $3.7 \pm 1.5\%$ compared with the radius determined by the electron scattering.

From the above results, one may conclude that for stable nuclei around $A/Z = 2$ the introduction of an almost energy-independent correction factor in the Glauber-type calculation can satisfactorily reproduce the measured σ_{cc}. This might suggest that the proton distributions (point-proton radii) of heavy ions can be derived from their charge-changing cross sections despite their different nuclear structures. As stated by Bhagwat and Gambhir [13], the correction factor may simply scale as a function of Z^2/N^2 in this energy range. Further experimental and theoretical investigations using unstable nuclei that have different A/Z and known charge radii would therefore be of great interest.

IV. SUMMARY

At intermediate energies, the charge-changing cross sections of heavy ions were proposed as a probe of their proton distributions. To test this hypothesis, we performed precision measurements of charge-changing cross sections of ^{28}Si on a carbon target in the energy range 100–600 MeV/nucleon, using high-precision data of the ^{28}Si charge distribution from a recent muonic x-ray experiment.

Together with data from the literature, the present experimental results clearly display a detailed energy dependence of the charge-changing cross sections in this energy range. Similar to the energy dependence of the total reaction cross sections for heavy ions, the charge-changing cross sections increase as the energy decreases below 200 MeV/nucleon and are almost constant over the range 200–600 MeV/nucleon.

A zero-range optical-limit Glauber-type calculation was performed and compared with the data. To reproduce the experimental data, a correction factor was introduced in the Glauber-type calculation. The factor takes into account the cross effects of the proton and neutron distributions of the projectile and shows an almost energy-independent enhancement by $\sim$12%. The present method can also reproduce the experimental charge-changing cross sections of other stable isotopes whose charge distributions are determined by electron scattering and muon capture experiments. The difference between experimental and predicted values is approximately 4% for isotopes around $A/Z = 2$. To test the applicability of the present method, a similar experimental investigation, probing different A/Z ratios, would be very interesting.

ACKNOWLEDGMENTS

The authors thank the AEC staff for their technical support and excellent accelerator operations. This work was supported by the Research Project with Heavy Ions at NIRS-HIMAC. M. Lantz acknowledges financial support from JSPS. We thank Dr. J. Miller at LBNL for his careful reading of this manuscript.

[1] H. Iwase, K. Niita, and T. Nakamura, J. Nucl. Sci. Technol. **39**, 1142 (2002).
[2] W. R. Webber, J. C. Kish, and D. A. Schrier, Phys. Rev. C **41**, 520 (1990).
[3] W. R. Webber, J. C. Kish, J. M. Rockstroh, Y. Cassagnou, R. Legrain, A. Soutoul, O. Testard, and C. Tull, Astrophys. J. **508**, 940 (1998).
[4] C. Zeitlin, S. Guetersloh, L. Heilbronn, J. Miller, A. Fukumura, Y. Iwata, T. Murakami, L. Sihver, and D. Mancusi, Phys. Rev. C **77**, 034605 (2008).
[5] C. Scheidenberger *et al.*, Phys. Rev. Lett. **88**, 042301 (2002).
[6] L. V. Chulkov *et al.*, Nucl. Phys. A **674**, 330 (2000).
[7] J. Meng, S.-G. Zhou, and I. Tanihata, Phys. Lett. B **532**, 209 (2002).
[8] O. V. Bochkarev *et al.*, Eur. Phys. J. A **1**, 15 (1998).
[9] M. Kanazawa *et al.*, Nucl. Phys. A **746**, 393c (2004).
[10] C. Zeitlin, A. Fukumura, S. B. Guetersloh, L. H. Heilbronn, Y. Iwata, J. Miller, and T. Murakami, Nucl. Phys. A **784**, 341 (2007).
[11] F. Flesch, G. Iancu, W. Heinrich, and H. Yasuda, Radiat. Meas. **34**, 237 (2001).
[12] R. J. Glauber, Lect. Theor. Phys. **1**, 315 (1959).
[13] A. Bhagwat and Y. K. Gambhir, Phys. Rev. C **69**, 014315 (2004).
[14] A. Ozawa *et al.*, Nucl. Phys. A **709**, 60 (2002); **727**, 465 (2003).
[15] G. Fricke, C. Bernhardt, K. Heilig, L. A. Schaller, L. Schellenberg, E. B. Shera, and C. W. De Jager, At. Data Nucl. Data Tables **60**, 177 (1995).
[16] L. C. Chamon, B. V. Carlson, L. R. Gasques, D. Pereira, C. De Conti, M. A. G. Alvarez, M. S. Hussein, M. A. Cândido Ribeiro, E. S. Rossi Jr., and C. P. Silva, Phys. Rev. C **66**, 014610 (2002).
[17] I. Sick, Phys. Lett. B **576**, 62 (2003).
[18] S. Kopecky, J. A. Harvey, N. W. Hill, M. Krenn, M. Pernicka, P. Riehs, and S. Steiner, Phys. Rev. C **56**, 2229 (1997).
[19] A. Ozawa, T. Suzuki, and I. Tanihata, Nucl. Phys. A **693**, 32 (2001).
[20] H. De Vries, C. W. De Jager, and C. De Vries, At. Data Nucl. Data Tables **36**, 495 (1987).
[21] A. N. Golovchenko, J. Skvarč, N. Yasuda, M. Giacomelli, S. P. Tretyakova, R. Ilić, R. Bimbot, M. Toulemonde, and T. Murakami, Phys. Rev. C **66**, 014609 (2002)
[22] I. Schall *et al.*, Nucl. Instrum. Methods Phys. Res. B **117**, 221 (1996).
[23] C. Zeitlin, S. Guetersloh, L. Heilbronn, J. Miller, A. Fukumura, Y. Iwata, and T. Murakami, Phys. Rev. C **76**, 014911 (2007).
[24] G. Iancu, F. Flesch, and W. Heinrich, Radiat. Meas. **39**, 525 (2005).